DYNAMICAL BEHAVIOUR OF A THREE-PHASE GENERATOR DUE TO UNBALANCED MAGNETIC PULL

Paolo Pennacchi
Dipartimento di Meccanica
Politecnico di Milano
Via La Masa, 34
I-20156 Milano, Italy
paolo.pennacchi@polimi.it

Lucia Frosini
Dipartimento di Ingegneria Elettica
Università degli studi di Pavia
Via Ferrata, 1
I-27100 Pavia, Italy
lucia@unipv.it

ABSTRACT

This paper presents a method to analyze the dynamical behaviour of large size generators due to the magnetic pull. In rotating electrical machines, the electromagnetic radial forces acting upon rotor and stator surfaces are very large, but they are balanced when the rotor is concentric with the stator. Similarly, the tangential forces produce only an axially rotating moment. If the rotor becomes eccentric, then an imbalance of these forces occurs, so that a net radial electromagnetic force, known as Unbalanced Magnetic Pull (UMP), is developed. The models traditionally proposed in the literature to study the UMP can be considered as reliable in case of small size electrical machines supported by rolling bearings. On the contrary, in case of large size machines, such as turbo-generators supported by oil-film bearings, the approximation of circular orbit for the geometric centre of the rotor is not acceptable. Nevertheless, the authors who have dealt with UMP in big size generators have disregarded that these rotor filtered orbits are elliptical and generally the orbit centre is not concentric with the stator.

A more realistic model is introduced in this work and the actual distribution of the air-gap length during the rotation will be determined in analytical terms, by taking into account the effects produced by the actual rotor orbit. The actual UMP is calculated by using the air-gap permeance approach and the simulation of the dynamical behaviour of a 320 MVA generator is presented, showing the harmonic content of the UMP and the presence of non-linearities.

INTRODUCTION

The motivation of the work arises from an industrial problem concerning two-poles turbo-generators of power plants. It is rather well known that the vibration spectrum of the generator itself has a relatively higher 2X harmonic component compared to the other parts of the shaft-line. The 2X vibrations can be caused by the radial stiffness asymmetry of the smooth two-poles generator due to the slots, by fluid-dynamics effects in the oil-film journal bearings and eventually by the magnetic pull. Moreover, some

faults that could occur in generators can excite also the 2X vibrations, as in the case of cracks. This fault is not so uncommon in generators (see [1]-[4]).

Since it is opportune to diagnose the presence of cracks in the incipient phase, the possibility to detect the 2X vibrations due to "natural" causes with respect to those due to the cracks is very important. Whilst some methods already exist in order to evaluate the effects due to the oil-film in the journal bearings and the radial asymmetry (that is however absent if the number of pole pairs is greater than one), non satisfactory models are available till now to study the magnetic pull in generators, that is due to rotor eccentricity.

Rotor eccentricity can occur in rotating electrical machines, as consequence of different causes (errors during assembly, bearings wear, bow of the shaft, etc.) or of the normal operating of a flexible machine. In rotating electrical machines, the electromagnetic radial forces acting upon rotor and stator surfaces are very large, but they are balanced when the rotor is concentric with the stator. Similarly, the tangential forces produce only an axially rotating moment.

If the rotor becomes eccentric, then an imbalance of these forces occurs, so that a net radial force is developed. This radial force, known as Unbalanced Magnetic Pull (UMP), causes vibrations and noise emission, speeds up the bearing wear and can even produce a rub between rotor and stator with a consequent damage of the stator windings.

Many researches have been addressed to this field since the 1960's, by developing specific problems or applications [5].

The works available in literature can be distinguished according to:

- the type of eccentricity (static or dynamic),
- the type of machine (induction, synchronous, brushless with permanent magnets, etc.),
- the type of studied effect (calculation of UMP, definition of fault indicators, modelling the dynamic behaviour of the machine).

The majority of the works in literature take into consideration the induction motors [6]-[16], mainly for two reasons: they are the most spread in industry (from small to large power) and their air-gaps are smaller than other machines (0.3-3 mm).

Recent works have been addressed to the study of eccentricity in:

- synchronous machines, which are normally used as generators of large power and can be with salient poles, with a "squat" rotor and a relative small air-gap (10-15 mm) [18] [19], or with smooth poles, with a "slim" rotor and a larger air-gap (30-100 mm) [20] [21];
- brushless motors with permanent magnets, which are used for small power in automation and robotics and have small air-gap (0.5 mm) [23] [24].

In this paper, the UMP in smooth poles generators is analyzed. Few papers are present in literature about these topics. In [20] a study is presented in which, despite of the fact that a 500 MVA, 3000 rpm generator is analyzed, rotor orbits are considered as circular. This can be a first approximation, since such kind of large machines are supported by oil-film bearings, whose anisotropy can hardly determine circular orbits.

Anyhow, the model presented shows that the resulting UMP has a constant component and a 2X harmonic component only.

In [21] some results presented in [13] for induction motors are used, and a simplified model with isotropic bearings (thus circular orbits) and a Jeffcott rotor is also presented. The approximate expression of the air-gap allows the authors to express the UMP in analytic closed form for different pole-pairs. Also in this case, for one pole-pair generator, the UMP has a constant component and a 2X harmonic component only. In [22] the results of [21] are used to study the stability of a 70 MVA hydro-generator, but the authors use a very simplified Euler-Bernoulli beam for the entire rotor.

The model presented in this paper introduces instead a very accurate calculation of the air-gap distribution depending on the position in a generic time instant of the rotor inside the stator. The air-gap length is then used to calculate the UMP by means of the air-gap permeance approach [13], that allows to obtain a closed form expression for the UMP, which is function of both time and position. In this way the UMP can be considered as an external forcing system acting on the rotor.

This method is applied to a model of a 320 MVA, 3000 rpm, 3-phase generator, which is modelled by means of standard finite beam elements normally used in rotor dynamics. The UMP is calculated for all the elements of the generator model that correspond to the slotted part. The Newmark method [25] is used to integrate the non linear dynamic equations of the system. The obtained results confirm the presence of the constant (not rotating) and 2X harmonic components of force but show the presence of a 1X component and of non-linear effects too.

As an alternative to the air-gap permeance approach, the finite element method could be used to model the electromagnetic system as well, as some authors have recently proposed in a study about induction motors [17]. The just quoted paper is somewhat mirrored in comparison with ours: in this case, a finite element model is used for the electromagnetic behaviour, while a very simple Jeffcott rotor model, with only 2 degrees of freedom and non-dimensional parameters, is employed for the mechanical behaviour.

It would be extremely interesting to employ finite element modelling for both mechanical and magnetic behaviours, but the calculation would require unacceptable computational times.

Moreover, since in the real machines it is generally simpler to measure the rotor vibrations in the bearings instead of the magnetic flux, a more accurate mechanical model of the generator could be preferable for industrial applications, as it could be validated by means of the measurements of the vibrations.

UMP MODELLING

Traditional models about UMP, which deal with the problem under an electrical point of view, normally present the distinction between static eccentricity and dynamic eccentricity. Using the electrical terminology, in the first case, the position of minimum radial length of the air-gap is fixed in the space: the rotor is symmetrical with respect to its axis and rotates about it. In the second case, the position of minimum

radial length of the air-gap rotates with the rotor: in case of a machine, which can be considered as rigid, the shaft axis does not coincide with the rotor axis (the rotor does not rotate about its axis).

The difference among static and dynamic eccentricity is actually relevant in case of electric motors of small to medium size in which very stiff bearing, normally rolling bearing, are used. The greater part of the available literature about UMP refers to these electric machines [9]-[16], in which very often the rotor is squat and can be considered as rigid or operates in any case below its first critical speed. Some other studies about generators [20] [21] present the same distinction that however is not so appropriate for high-speed turbo-generators: first, these machines operate over their first critical speed, therefore are flexible and present always the so called dynamic eccentricity; second, since oil-film bearing are used, the oil-film forces determine the rotor centreline to describe a path during the run-up, therefore the rotor centreline is not statically concentric with the stator, unless a specific alignment operation is performed.

Since this paper deals with high-speed turbo-generators, we do not consider the distinction between static and dynamic eccentricity and the air-gap length distribution is determined in the general case as a function of the position of the rotor in a general time instant with respect to the stator. Moreover, the dynamical deformation of the rotor produces an air-gap distribution that is not constant along the span of the rotor. For this reason, the air-gap distribution has to be defined for each section of the machine slotted part.

Let consider figure 1 in which the relative position of the rotor and the stator are shown in a general time instant t, for a generator section, and the average air-gap length is intentionally magnified for graphical clearness. The reference system $S'(x',\mathrm{O}',y')$ is fixed and centred in the stator centre O', while the reference system $S''(x'',\mathrm{O}'',y'')$ has its centre O'' that corresponds to the rotor centreline. Due to the presence of lateral vibrations, the rotor centre O describes an orbit around the centreline. Therefore, the eccentricity between the stator and the rotor centre is determined by two components: the offset $\overrightarrow{\mathrm{O}'\mathrm{O}''}$ due to the centreline path during the run-up and the lateral vibration $\overrightarrow{\mathrm{O}''\mathrm{O}}$ of the rotor. The position of the rotor centre $\mathrm{P}_0 \equiv \mathrm{O}$ in a general time instant t depends on the previous time history and on the exciting systems acting on the shaft. The reference system $S(x,\mathrm{O},y)$ is centred in the rotor centre. Since the aim is to determine the air-gap length radial distribution, the angular relative position of S and S' is not relevant and for simplicity the reference axes are considered as parallel.

The equations of the stator circumference $\Gamma_2^{(S)}$ in the reference S are in parametric form:

$$\Gamma_2^{(S)}:\begin{cases} x(t) = x_{\mathrm{O}'}(t) + r_s\cos\alpha \\ y(t) = y_{\mathrm{O}'}(t) + r_s\sin\alpha \end{cases}, 0 \le \alpha < 2\pi \tag{1}$$

and in implicit form:

$$\left(x - x_{\mathrm{O}'}\right)^2 + \left(y - y_{\mathrm{O}'}\right)^2 = r_s^2 \tag{2}$$

in which $\mathbf{x}_{O'} = x_{O'}(t)\mathbf{i} + y_{O'}(t)\mathbf{j}$ indicates the position vector of O' in the reference system S in a general time instant t. These values are actually the absolute vibration of rotor with respect to the stator centre. The equation of a general line $\Gamma_3^{(S)}$ in reference system S passing through P_0 is:

$$\Gamma_3^{(S)}: \ y = x\tan\beta, \ |\beta| \neq \frac{\pi}{2} \tag{3}$$

$$\Gamma_3^{(S)}: \ x = 0, \ |\beta| = \frac{\pi}{2} \tag{4}$$

The angle β is sometimes referred as *spatial angle* in Electrical Engineering literature. If $|\beta| \neq \frac{\pi}{2}$ the intersections $\{P_1, P_2\} = \Gamma_3 \cap \Gamma_2$ between the general line passing through P_0 and the stator are obtained by replacing eq. (3) in eq. (2):

$$\{P_1, P_2\}^{(S)}: \ \begin{cases} (x - x_{O'})^2 + (x\tan\beta - y_{O'})^2 = r_s^2 \\ y = x\tan\beta \end{cases}, \quad |\beta| \neq \frac{\pi}{2} \tag{5}$$

After some manipulation, first equation of eq. (5) becomes:

$$x^2 - 2x\left(x_{O'}\cos^2\beta + y_{O'}\cos\beta\sin\beta\right) - r_s^2\cos^2\beta + x_{O'}^2\cos^2\beta + y_{O'}^2\cos^2\beta = 0 \tag{6}$$

Eq. (6) is a 2nd order algebraic equation in the unknown x and has two solutions: that with + sign corresponds to intersection points for $|\beta| < \frac{\pi}{2}$, like point P_1 in figure 1, while that with – sign to intersection points for $-\pi < \beta < -\frac{\pi}{2} \cup \frac{\pi}{2} < \beta \leq \pi$, like point P_2 in figure 1. After some simplifications, co-ordinates of points P_1 and P_2 result:

$$\{P_1, P_2\}^{(S)}: \ \begin{cases} x_{P_1,P_2} = x_{O'}\cos^2\beta + y_{O'}\cos\beta\sin\beta \pm \sqrt{\cos^2\beta\left(r_s^2 - \left(y_{O'}\cos\beta - x_{O'}\sin\beta\right)^2\right)} \\ y_{P_1,P_2} = x_{O'}\cos\beta\sin\beta + y_{O'}\sin^2\beta \pm \tan\beta\sqrt{\cos^2\beta\left(r_s^2 - \left(y_{O'}\cos\beta - x_{O'}\sin\beta\right)^2\right)} \end{cases}, \quad |\beta| \neq \frac{\pi}{2} \tag{7}$$

In the special case $|\beta| = \frac{\pi}{2}$, the intersections $\{P_1, P_2\} = \Gamma_3 \cap \Gamma_2$ are obtained by replacing eq. (4) in eq. (2):

$$\{P_1, P_2\}^{(S)}: \ \begin{cases} x_{O'}^2 + (y - y_{O'})^2 = r_s^2 \\ x = 0 \end{cases}, \quad |\beta| = \frac{\pi}{2} \tag{8}$$

and finally:

$$\{\mathrm{P}_1,\mathrm{P}_2\}^{(S)}:\quad \begin{cases} x_{\mathrm{P}_1,\mathrm{P}_2}=0 \\ y_{\mathrm{P}_1,\mathrm{P}_2}=y_{\mathrm{O}'}\pm\sqrt{r_s^2-x_{\mathrm{O}'}^2} \end{cases},\quad |\beta|=\frac{\pi}{2} \tag{9}$$

The equations of the rotor circumference $\Gamma_1^{(S)}$ in the reference S are in parametric form:

$$\Gamma_1^{(S)}:\begin{cases} x=r_r\cos\gamma \\ y=r_r\sin\gamma \end{cases},\ 0\le\gamma<2\pi \tag{10}$$

and in implicit form:

$$x^2+y^2=r_r^2 \tag{11}$$

If the spatial angle $|\beta|\neq\frac{\pi}{2}$, the intersections $\{\mathrm{P}_3,\mathrm{P}_4\}=\Gamma_3\cap\Gamma_1$ between the general line passing through P_0 and the rotor are given replacing eq. (3) in eq. (11):

$$\{\mathrm{P}_3,\mathrm{P}_4\}^{(S)}:\quad \begin{cases} x^2+y^2=r_r^2 \\ y=x\tan\beta \end{cases},\quad |\beta|\neq\frac{\pi}{2} \tag{12}$$

After some manipulation, first equation of eq. (12) becomes:

$$x^2-r_r^2\cos^2\beta=0 \tag{13}$$

Eq. (13) has two solutions: that with $+$ sign corresponds to intersection points for $|\beta|<\frac{\pi}{2}$, like point P_3 in figure 1, while that with $-$ sign to intersection points for $-\pi<\beta<-\frac{\pi}{2}\cup\frac{\pi}{2}<\beta\le\pi$, like point P_4 in figure 1. After some simplifications, co-ordinates of points P_3 and P_4 result simply:

$$\{\mathrm{P}_3,\mathrm{P}_4\}^{(S)}:\quad \begin{cases} x_{\mathrm{P}_3,\mathrm{P}_4}=\pm r_r^2\cos\beta \\ y_{\mathrm{P}_1,\mathrm{P}_2}=\pm r_r^2\sin\beta \end{cases},\quad |\beta|\neq\frac{\pi}{2} \tag{14}$$

For $|\beta|=\frac{\pi}{2}$, the co-ordinates of points P_3 and P_4 are purely:

$$\{\mathrm{P}_3,\mathrm{P}_4\}^{(S)}:\quad \begin{cases} x_{\mathrm{P}_3,\mathrm{P}_4}=0 \\ y_{\mathrm{P}_1,\mathrm{P}_2}=\pm r_r \end{cases},\quad |\beta|=\frac{\pi}{2} \tag{15}$$

Finally, the air-gap length $\delta(\mathbf{x}_{\mathrm{O}'},\beta,t)$ is given by the distance between points P_1 and P_3 for $|\beta|<\frac{\pi}{2}\cup\beta=\frac{\pi}{2}$ and between points P_2 and P_4 for $-\pi<\beta\le-\frac{\pi}{2}\cup\frac{\pi}{2}<\beta\le\pi$ respectively:

$$\delta\left(\mathbf{x}_{\mathrm{O}'},\beta,t\right)=\sqrt{\left(x_{\mathrm{P}_1,\mathrm{P}_2}-x_{\mathrm{P}_3,\mathrm{P}_4}\right)^2+\left(y_{\mathrm{P}_1,\mathrm{P}_2}-y_{\mathrm{P}_3,\mathrm{P}_4}\right)^2} \tag{16}$$

The closed form of the air-gap length $\delta\left(\mathbf{x}_{\mathrm{O}'},\beta,t\right)$, after some algebra, is:

$$\delta_{rh}\left(\mathbf{x}_{\mathrm{O}'},\beta,t\right)=\left(\begin{array}{l} r_s^2+r_r^2+x_{\mathrm{O}'}^2\cos 2\beta+4x_{\mathrm{O}'}y_{\mathrm{O}'}\cos\beta\sin\beta-y_{\mathrm{O}'}^2\cos 2\beta- \\ -2r_r\left(x_{\mathrm{O}'}\cos\beta+y_{\mathrm{O}'}\sin\beta\right)+ \\ +2\left(x_{\mathrm{O}'}+y_{\mathrm{O}'}\tan\beta-r_r\sec\beta\right)\sqrt{\cos^2\beta\left(r_s^2-\left(x_{\mathrm{O}'}\sin\beta-y_{\mathrm{O}'}\cos\beta\right)^2\right)} \end{array}\right)^{1/2} \tag{17}$$

if the spatial angle satisfies the condition $|\beta|<\dfrac{\pi}{2}$, otherwise is:

$$\delta_{lt}\left(\mathbf{x}_{\mathrm{O}'},\beta,t\right)=\left(\begin{array}{l} r_s^2+r_r^2+x_{\mathrm{O}'}^2\cos 2\beta+4x_{\mathrm{O}'}y_{\mathrm{O}'}\cos\beta\sin\beta-y_{\mathrm{O}'}^2\cos 2\beta+ \\ +2r_r\left(x_{\mathrm{O}'}\cos\beta+y_{\mathrm{O}'}\sin\beta\right)- \\ -2\left(x_{\mathrm{O}'}+y_{\mathrm{O}'}\tan\beta+r_r\sec\beta\right)\sqrt{\cos^2\beta\left(r_s^2-\left(x_{\mathrm{O}'}\sin\beta-y_{\mathrm{O}'}\cos\beta\right)^2\right)} \end{array}\right)^{1/2} \tag{18}$$

if $-\pi<\beta<-\dfrac{\pi}{2}\cup\dfrac{\pi}{2}<\beta\le\pi$ and finally is:

$$\delta_{v}\left(\mathbf{x}_{\mathrm{O}'},\beta,t\right)=\left|y_{\mathrm{O}'}\pm\sqrt{r_s^2-x_{\mathrm{O}'}^2}\pm r_r\right| \tag{19}$$

if $|\beta|=\dfrac{\pi}{2}$.

It is possible to show that the air-gap length $\delta\left(\mathbf{x}_{\mathrm{O}'},\beta,t\right)$ eqs. (17) and (18) can be estimated by means of the approximated formula given by [20] [21] if the orbit is circular and its centre is concentric with the stator, i.e. $\mathrm{O}''\equiv\mathrm{O}'$.

In order to calculate the radial force due to the UMP on a general element *j*-th of the rotor, once that the spatial air-gap length distribution is known with respect to the considered rotor element and the stator, the Maxwell stress tensor is used:

$$\begin{aligned}\sigma_r&=\frac{1}{2\mu_0}\left(B_r^2-B_\theta^2\right)\\ \sigma_\theta&=\frac{1}{\mu_0}B_r B_\theta\end{aligned} \tag{20}$$

where the subscript r indicates the radial component and θ the tangential component, B is the air-gap flux density and μ_0 is the vacuum magnetic permeability. It is generally commonly accepted that the tangential

component is negligible, as done in [11] [20] [21]. This is a rather acceptable approximation only for concentric rotors. In case of eccentric rotors this is less reliable, but there are some studies, even if related to cage induction motors [7], that suggest that is reasonable to neglect the tangential stress, providing that large eccentricities are avoided. Therefore, for simplicity it is assumed that $B_\theta = 0$, taking also into account that the method is proposed to study the lateral vibrations of the generator and that in the finite element model used in the follow the torsional degree of freedom is neglected.

The magnetic flux $\mathbf{\Phi}_r$ that cross radially the air-gap is given by:

$$\mathbf{\Phi}_r = \mathbf{M}\Lambda \tag{21}$$

where $\mathbf{M}$ is the magnetomotive force due to the interaction of the rotor and stator magnetic fields produced by the winding currents of one pole-pair and Λ is the permeance of the magnetic circuit carrying the magnetic flux $\mathbf{\Phi}_r$.

As first approximation, since the permeance of the air-gap is much smaller than the permeance of the rotor and stator iron core, the last is neglected in the calculation of the magnetomotive force $\mathbf{M}$:

$$\mathbf{M} = \frac{\mathbf{\Phi}_r}{\Lambda} = \frac{\mathbf{B}_r \bar{S}}{\frac{\mu_0 \bar{S}}{2\delta}} = \frac{2\mathbf{B}_r \delta}{\mu_0} \tag{22}$$

where $\bar{S}$ is any normal surface crossed by the magnetic flux. For a more accurate calculation, it could be take into account that:

- the actual length of the air-gap feels the effects of the stator and rotor slots; therefore its value, and consequently the value of the magnitude of the magnetomotive force $\mathbf{M}$ obtained by eq. (22), has to be multiplied by the Carter factor $k_C = 1 \div 1.1$ [26];
- the reluctance of the iron core is not completely negligible. In case of a smooth rotor machine, the iron core consists of the stator yoke, the rotor yoke and the stator and rotor teeth. The magnetomotive force needed to establish the flux in the iron core is calculated by means of the magnetization curve of the material and depends on the values assumed by the flux density in the different iron parts. The larger contribution is given by the stator and rotor teeth, because in these parts the value of flux density is considerably greater than in the air-gap (1.8÷2 times).

As well known, the magnetization curve of the ferromagnetic material shows an almost linear behaviour with high slope until a certain value of the flux density: in this part of the curve the relative magnetic permeability of the material is very high (in the order of the thousands) and consequently the reluctance of the iron core is much smaller (nearly negligible) than the reluctance of the air-gap. When the flux density exceeds that value, the magnetic saturation happens: the slope of the curve decreases so much that the relative permeability of the material assumes values comparable to the air.

So, in order to avoid the saturation in the iron teeth, it is necessary to impose the maximum value of the flux density B_r in the range 0.6÷1 T, with highest values for large power machines.

On open circuit (at no-load), i.e. when the machine does not supply electric power, the magnetomotive force is due solely to the direct current of the rotor field windings and shows a sinusoidal spatial distribution around the air-gap with period twice the pole pitch τ :

$$\tau = \frac{\pi R}{p_p} \tag{23}$$

where R is the mean air-gap radius and p_p the number of pole-pairs. In fact, the mean air-gap length δ is small compared to the mean air-gap radius R, therefore $R \cong r_s \cong r_r$.

Since the rotor rotates at speed ω_r :

$$\omega_r = \frac{2\pi f_s}{p_p} \tag{24}$$

where f_s is the supply frequency, it follows that the magnetomotive force on open circuit $\mathbf{M}_0$ is variable during the time. For the Faraday-Lenz law, the magnetic flux on open circuit $\mathbf{\Phi}_0$ produced by $\mathbf{M}_0$ induces an electromotive force $\mathbf{V}_0$ in each phase of the stator armature winding.

Since the maximum value of the flux density B_r is fixed, with equal dimensions of the machine and equal number of pole pairs, it follows that also the rms value of the magnetic flux on open circuit $\hat{\Phi}_0$ is fixed. Moreover, since the generator must work at the nominal voltage $\hat{V}_n$ fixed by the power grid, even the rms value of the electromotive force $\hat{V}_0$ is fixed equal to $\hat{V}_n$.

The induced electromotive force $\mathbf{V}_0$ is proportional to the derivative with respect to time of the flux $\mathbf{\Phi}_0$ by means of a constant which depends on the number of stator conductors per phase: this number is therefore determined on the basis of the fixed values of $\hat{\Phi}_0$, f_s and $\hat{V}_n$.

The magnetomotive force on open circuit $\mathbf{M}_0$, responsible for the production of the flux $\mathbf{\Phi}_0$, can be calculated as first approximation by means of eq. (22). It is produced by the field currents that circulate in the $2N_r$ coils of a rotor pole-pair. Since the rotor conductors carry a direct current, the sinusoidal waveform of the magnetomotive force is obtained by means of an appropriate distributed winding [26] and its rms value can be expressed by the following equation:

$$\hat{M}_0 \equiv \hat{M}_{r0} = 2N_r \hat{I}_{r0} \tag{25}$$

where $\hat{I}_{r0}$ represents a rms value of the sinusoidal distribution of the direct current in the rotor slots.

When the generator is connected to the power grid, the three-phase stator windings carry a balanced set of sinusoidal alternating currents which establish a rotating magnetic field defined by the vector $\mathbf{B}_{rs}$. This phenomenon, known as "armature reaction", modifies the magnetic flux on open circuit $\mathbf{\Phi}_0$ produced by the rotor magnetic field $\mathbf{B}_{rr}$. The resultant air-gap magnetic field $\mathbf{B}_r$ is given by the vectorial sum $\mathbf{B}_r = \mathbf{B}_{rr} + \mathbf{B}_{rs}$ [27] [28]. In this situation, if the field currents that produce the rotor field $\mathbf{B}_{rr}$ are not modified, the rms value of the electromotive force $\hat{V}_i$ induced in the stator windings will no more equal to $\hat{V}_n$. In the common case of resistive-inductive load, the effect of the armature reaction is to reduce the air-gap magnetic field and, as consequence, to decrease the electromotive force induced in the stator windings.
Therefore, in case of resistive-inductive load, the field current has to be increased in order to make up for the reduction of the air-gap flux caused by the armature reaction:

$$\hat{M}_{rload} = 2N_r\hat{I}_{rload} > \hat{M}_{r0} = 2N_r\hat{I}_{r0} \tag{26}$$

The magnetomotive force at load $\mathbf{M}_{load}$, responsible to establish the air-gap flux $\mathbf{\Phi}_0$, will not vary with respect to the magnetomotive force on open circuit $\mathbf{M}_0$:

$$\hat{M}_{load} = \hat{M}_{rload} - \hat{M}_{sload} = 2N_r\hat{I}_{rload} - \hat{M}_{sload} = \hat{M}_0 \tag{27}$$

On the basis of these considerations, the following calculations related to the air-gap field $\mathbf{B}_r$ would be valid in both load and no-load conditions.

Nevertheless, in load condition, it is necessary to consider that the terminal voltage $\hat{V}_{ph}$ on each phase of the stator armature winding is not equal to the induced electromotive force $\hat{V}_i$, but differs from that for the fall of voltage $\Delta\hat{V}$ due to the losses for Joule effect and leakage flux.

Therefore, in order to maintain in load condition the terminal voltage $\hat{V}_{ph}$ constant and equal to the nominal voltage $\hat{V}_n$ fixed by the power grid, the magnetomotive force $\mathbf{M}_{load}$ must produce an air-gap magnetic flux greater than the open circuit flux $\mathbf{\Phi}_0$; in this way the flux will be able to induce an electromotive force $\hat{V}_i = \hat{V}_n + \Delta\hat{V}$.

As consequence, even the maximum value of the air-gap flux density will be greater in load operation compared to the open circuit condition, e.g. if $B_{r0} = 1\ \mathrm{T}$, $B_{rload} = 1.1 \div 1.2\ \mathrm{T}$.

In any case, during both load and no-load operations, the magnetomotive force $\mathbf{M}$ establishing the air-gap magnetic flux $\mathbf{\Phi}_r$ can be expressed as a Fourier series: its first harmonic component has a sinusoidal spatial

distribution through the air-gap with period twice the pole pitch τ and its amplitude is sinusoidally variable during the time, depending on the supply frequency f_s:

$$\mathbf{M}_1(z,t) = \bar{M}_1 \cos\left(\omega t - \frac{\pi z}{\tau}\right) = \bar{M}_1 \cos\left(\omega t - \frac{\pi z}{\frac{\pi R}{p_p}}\right) = \bar{M}_1 \cos\left(\omega t - p_p \frac{z}{R}\right) \tag{28}$$

where $\omega = 2\pi f_s$, z is the distance around the air-gap from a reference point and $\frac{z}{R} = \beta$.

By considering for simplicity only the first harmonic component of the magnetomotive force per each pole, the air-gap flux density becomes:

$$\mathbf{B}_r(\mathbf{x}_{O'}, \beta, t) = \mu_0 \frac{\mathbf{M}_1(\beta,t)/2}{\delta(\mathbf{x}_{O'}, \beta, t)} = \mu_0 \frac{\bar{M}_1 \cos(\omega t - p_p \beta)/2}{\delta(\mathbf{x}_{O'}, \beta, t)} \tag{29}$$

where the $\delta(\mathbf{x}_{O'}, \beta, t)$ is the actual air-gap length distribution calculated in eqs. (17)-(18). By using eq. (29) in eq. (20), the Maxwell stress becomes:

$$\sigma_r(\mathbf{x}_{O'}, \beta, t) = \frac{B_r^2(\mathbf{x}_{O'}, \beta, t)}{2\mu_0} = \mu_0 \frac{M_1^2(\beta,t)}{8\delta^2(\mathbf{x}_{O'}, \beta, t)} = \frac{\mu_0 \bar{M}_1^2}{8} \frac{\cos^2(\omega t - p_p \beta)}{\delta^2(\mathbf{x}_{O'}, \beta, t)} \tag{30}$$

The resultant forces, due to the UMP, on the considered element *j*-th of the rotor, in horizontal and vertical direction, are finally obtained by integrating Maxwell stress along the spatial angle of eq. (30):

$$\begin{aligned} F_{x,UMP}^{(j)}(\mathbf{x}_{O'}, t) &= \int_0^{2\pi} \sigma_r(\mathbf{x}_{O'}, \beta, t) r_r^{(j)} l^{(j)} \cos\beta d\beta = \\ &= \frac{\mu_0 \bar{M}_1^2}{8} r_r^{(j)} l^{(j)} \left(\int_{-\pi/2}^{\pi/2} \frac{\cos\beta \cos^2(\omega t - p_p \beta)}{\delta_{rh}^2(\mathbf{x}_{O'}, \beta, t)} d\beta + \int_{\pi/2}^{3\pi/2} \frac{\cos\beta \cos^2(\omega t - p_p \beta)}{\delta_{lt}^2(\mathbf{x}_{O'}, \beta, t)} d\beta \right) \end{aligned} \tag{31}$$

$$\begin{aligned} F_{y,UMP}^{(j)}(\mathbf{x}_{O'}, t) &= \int_0^{2\pi} \sigma_r(\mathbf{x}_{O'}, \beta, t) r_r^{(j)} l^{(j)} \sin\beta d\beta = \\ &= \frac{\mu_0 \bar{M}_1^2}{8} r_r^{(j)} l^{(j)} \left(\int_{-\pi/2}^{\pi/2} \frac{\sin\beta \cos^2(\omega t - p_p \beta)}{\delta_{rh}^2(\mathbf{x}_{O'}, \beta, t)} d\beta + \int_{\pi/2}^{3\pi/2} \frac{\sin\beta \cos^2(\omega t - p_p \beta)}{\delta_{lt}^2(\mathbf{x}_{O'}, \beta, t)} d\beta \right) \end{aligned} \tag{32}$$

where $r_r^{(j)}$ and $l^{(j)}$ are respectively the radius and the length of the element *j*-th of the rotor.

APPLICATION TO A ROTATING MACHINE

In order to evaluate the dynamical effects of the UMP in rotating machinery, the method described in the previous chapter is applied to the model of a 320 MVA smooth poles 3-phase generator with its exciter. For simplicity, only the generator model is considered and the turbine parts of the shaft line of the turbo-generator system are omitted. The considered machine operates at 3000 rpm, the supply frequency is 50 Hz (being the generator a synchronous machine) and has only one pole-pair. Due to its design, this type of generator presents polar stiffness asymmetry that can cause by itself 2X vibration component [29] [30] [31]. Anyhow this fact is not considered and modelled here in order not to mask the 2X vibration due to UMP.

The rotor is modelled by means of a finite element model with 33 beam element, with 4 degrees of freedom (d.o.f.s) per node, and is supported by three oil-film bearings (figure 2). The generator slotted part corresponds to the beam elements 16, 17, 18 and 19 (figure 7).

The general *j*-th rotor element d.o.f.s (generalized displacements, see figure 3) are ordered as:

$$\mathbf{x}^{(j)} = \left\{ x_j \quad \vartheta_{x_j} \quad y_j \quad \vartheta_{y_j} \quad x_{j+1} \quad \vartheta_{x_{j+1}} \quad y_{j+1} \quad \vartheta_{y_{j+1}} \right\}^{\mathrm{T}} \tag{33}$$

Even if the oil-film forces are not constant and depend, among other causes, on the loads on the bearings, in order to evaluate only the effects of the UMP, they are considered constant and linearized damping and stiffness coefficients are used. This simplification allows not to integrate Reynolds equation and not to introduce non-linearities that can mask possible similar effects caused by the UMP. This fact implies also that the journal eccentricity and attitude angle due to oil-film forces (and centreline position too) are not changing at the end of the run-up to the operating speed.

Bearing #1 and #2 are elliptical and equal, while bearing #3 is of tilting-pad type. The linearized coefficients employed for the simulation are calculated at the operating speed using reference [32] and are reported in table 1 (subscript *x* indicates horizontal direction and *y* vertical direction).

Table 1 Linearized dynamic coefficients for the bearings.

	k_{yy}	k_{yx}	k_{xy}	k_{xx}	r_{yy}	r_{yx}	r_{xy}	r_{xx}
Brg. #1	1.00e9	–7.00e8	1.20e8	6.00e8	2.00e7	–1.00e7	–1.00e7	2.00e7
Brg. #2	1.00e9	–7.00e8	1.20e8	6.00e8	2.00e7	–1.00e7	–1.00e7	2.00e7
Brg. #3	8.00e7	0	0	8.00e7	2.00e6	0	0	2.00e6

The supporting structure is modelled by means of pedestals. The fully assembled system (rotor + bearings + foundation) mass matrix - which takes also into account the secondary effect of the rotatory inertia -, the damping matrix, the stiffness matrix - which takes also into account the shear effect - and the gyroscopic matrix can be defined by means of standard Lagrange's methods for beam elements as shown e.g. in [33], while the assembly of the total system (rotor, bearings and supporting structure) equations can be done by following the method described in [34]:

$$[\mathbf{M}]\ddot{\mathbf{x}}+[\mathbf{C}]\dot{\mathbf{x}}+[\mathbf{K}]\mathbf{x}=\mathbf{F}(\mathbf{x},t) \tag{34}$$

where $[\mathbf{M}]$ is the mass matrix, $[\mathbf{C}]$ is the damping matrix, which includes also the gyroscopic matrix calculated at the operating speed, $[\mathbf{K}]$ is the stiffness matrix. Note that in eq. (34) the translational components x and y of the node vibrations $\mathbf{x}$ are relative to the centreline of the rotor O'', while the part of the external exciting force $\mathbf{F}(\mathbf{x},t)$ due to the UMP depends on the relative position $\mathbf{x}_{\mathrm{O}'}$ of the rotor centre P_0 with respect to the stator centre O' (see figure 4). In fact, the actual air-gap length distribution depends on the relative position between the stator and the rotor as shown in eqs. (17) and (18).

In other terms, if ξ and η are the rotor offsets, due to oil-film forces, in horizontal and vertical direction, which are considered as constant, due to the centreline path during the run-up:

$$(\mathrm{P}_0-\mathrm{O}'')=(\mathrm{O}'-\mathrm{O}'')+(\mathrm{P}_0-\mathrm{O}')\rightarrow\begin{cases}x_{\mathrm{O}'}=x\pm\xi\\ y_{\mathrm{O}'}=y\pm\eta\end{cases} \tag{35}$$

where the sign $+$ or $-$ depends on the relative position of O' and O''.

The modal analysis of the generator alone, performed at the operating speed of 3000 rpm shows that it has three eigenfrequencies below 50 Hz, namely 13.07, 39.03 and 43.62 Hz. The corresponding modes are shown in figure 5 (stiffness diameters are used for the rotor sketch).

It is worthy to note that the generator has also two other modes over 50 Hz, which could be excited by the UMP, whose eigenfrequencies are 83.21 and 100.04 Hz. Anyhow, the modal deformation at about 100 Hz is very reduced in the generator slotted part, therefore a 2X excitation due to UMP, being applied on this rotor part, is expected to be not very effective on the system response.

The external exciting force vector $\mathbf{F}(\mathbf{x},t)$ of eq. (34) includes the original unbalance of the rotor and the effect of the UMP. Moreover, the UMP acting on a rotor element, is applied into the first node of the element, even if it is calculated using the element span. Then, if for simplicity the node of application of the unbalance does not correspond to any node of application of UMP, the structure of the column vector $\mathbf{F}(\mathbf{x},t)$ is typically:

$$\mathbf{F}(\mathbf{x},t)=\Big\{\vdots\ \underbrace{me\omega^2\cos\omega t\quad 0\quad me\omega^2\sin\omega t\quad 0}_{\text{rotor node in which the unbalance is applied}}\ \vdots\ \underbrace{F_{x,UMP}^{(k)}\quad 0\quad F_{y,UMP}^{(k)}\quad 0}_{\text{first node of an element in which the UMP is applied}}\ \vdots\ \underbrace{0\quad\cdots\quad 0}_{\text{foundation d.o.f.s}}\Big\}^{\mathrm{T}} \tag{36}$$

If the node of application of the unbalance coincides with an application node of the UMP, then superposition of the two effects is used.

The non-linear system of equations in eq. (34) is integrated using the Newmark implicit method, in which the forcing vector of eq. (36) is recalculated at each time step: the UMP forces are calculated using eqs. (31)

and (32) considering the air-gap distribution due to the vibration at the previous time step. Actually, Newmark method would require that the UMP forces where those of the current time step, but they can be calculated only for the air-gap length distribution at the previous time step. Anyhow, if Δt is small, the differences between $\mathbf{F}(\mathbf{x}_{i-1}, t_i)$ and $\mathbf{F}(\mathbf{x}_i, t_i)$ are negligible. The algorithm is the following:

1. Starting from a suitable set of initial conditions $\mathbf{x}_0$ and $\dot{\mathbf{x}}_0$ for $t = 0$, the force vector $\mathbf{F}(\mathbf{x}_0, 0)$ is calculated, using eqs. (31) and (32) for the UMP part.
2. The initial acceleration vector is calculated by:

$$\ddot{\mathbf{x}}_0 = [\mathbf{M}]^{-1}\left(\mathbf{F}(\mathbf{x}_0, 0) - [\mathbf{C}]\dot{\mathbf{x}}_0 - [\mathbf{K}]\mathbf{x}_0\right) \tag{37}$$

3. Starting from the first time step, in a general time step *i*-th, the new force vector $\mathbf{F}(\mathbf{x}_{i-1}, t_i)$ is calculated and the generalized displacements, accelerations and velocities are equal to:

$$\mathbf{x}_i = \left[\frac{1}{a\,\Delta t^2}[\mathbf{M}] + \frac{b}{a\,\Delta t}[\mathbf{C}] + [\mathbf{K}]\right]^{-1} \left(\begin{array}{l} \mathbf{F}(\mathbf{x}_{i-1}, t_i) + \left[\frac{1}{a\,\Delta t^2}[\mathbf{M}] + \frac{b}{a\,\Delta t}[\mathbf{C}]\right]\mathbf{x}_{i-1} + \\ + \left[\frac{1}{a\,\Delta t}[\mathbf{M}] - \left(1 - \frac{b}{a}\right)[\mathbf{C}]\right]\dot{\mathbf{x}}_{i-1} + \\ + \left[\frac{1}{a}\left(\frac{1}{2} - a\right)[\mathbf{M}] - \Delta t\left(1 - \frac{b}{2\,a}\right)[\mathbf{C}]\right]\ddot{\mathbf{x}}_{i-1} \end{array} \right) \tag{38}$$

$$\ddot{\mathbf{x}}_i = \frac{1}{a\,\Delta t^2}\left(\mathbf{x}_i - \mathbf{x}_{i-1} - \dot{\mathbf{x}}_{i-1}\Delta t\right) - \frac{1}{a}\left(\frac{1}{2} - a\right)\ddot{\mathbf{x}}_{i-1} \tag{39}$$

$$\dot{\mathbf{x}}_i = \frac{b}{a\,\Delta t}\left(\mathbf{x}_i - \mathbf{x}_{i-1}\right) + \left(1 - \frac{b}{a}\right)\dot{\mathbf{x}}_{i-1} + \Delta t\left(1 - \frac{b}{2\,a}\right)\ddot{\mathbf{x}}_{i-1} \tag{40}$$

The constants a and b of the Newmark method are assumed respectively equal to 0.25 and 0.5, which is equivalent to the "trapezium rule" and assures that the implicit integration is unconditionally stable, without adding numerical spurious damping (high values of b). In fact it can be proven that Newmark method is unconditionally stable if $b \geq 0.5$ and $a \geq 0.25(0.5 + b)^2$.

NUMERICAL RESULTS

The methods presented in the previous chapters have been applied to the considered model of the generator. Only the central part of the generator, that corresponding to the slotted part, namely elements 16, 17, 18 and 19, is relevant for the calculation of the UMP forces (figure 7). The diameter of these elements is 1024 mm. The nominal air-gap length is generally 60 mm for generators of this size. In order to carry on with the simulation, it is necessary to calculate a first approximation value for $\bar{M}_1$, neglecting the effect of the slots,

the iron core reluctance and the voltage fall. Starting from eq. (22), we can impose $B_r = 1\,\mathrm{T}$ and $\delta = 0.06\,\mathrm{m}$:

$$\frac{\bar{M}_1}{2} = \frac{B_r \delta}{\mu_0} = \frac{1 \cdot 0.06}{4\pi \cdot 10^{-7}} \cong 47746\ \mathrm{A} \tag{41}$$

This approximation is not relevant for the simulation, since the value of eq. (41) is simply increased taking into account the previous effects. If we consider seven coils per pole, each with a square section of 40×40 mm^2, the current density is 4.26 A/mm^2, that is rather acceptable.

Once again, it should also be considered that in these machines, due to the presence of the anisotropy of the oil-film bearings, the centreline position is affected significantly by the geometry of the oil-film inside the bearing. Even without considering any other external forcing system, except oil-film forces and the weight, the journal assumes an attitude angle and is eccentric with respect to the bearing case. Since, for simplicity, oil-film forces are considered as constant at the operating speed, this fact causes a constant offset for each bearing. Even if the offset is not equal for all the bearings of the machine nor for each element with respect to the case and the stator, it is possible to consider a common offset for all of them without loosing the soundness of the results. Therefore the rotor centreline is considered to have an eccentric offset of ξ = 50 μm in horizontal negative direction and η = 200 μm in vertical negative direction with respect to the stator centre (Figure 4). These offsets are used in eq. (35) along to the vibrations of the nodes in order to calculate the absolute vibrations of rotor with respect to the stator centre and then the air-gap length distribution and the UMP. Finally, an unbalance, simulating the residual unbalance of the machine, with amplitude of 1 kgm was applied on node 17.

For the selection of the initial conditions, a first simulation of 1 s was performed neglecting the presence of the UMP and starting from a null displacement $\mathbf{x}_0 = 0$ and velocity $\dot{\mathbf{x}}_0 = 0$ vector. After an initial very chaotic motion, the node orbits tends to become stable and the displacement and velocity vectors of the last time step are stored as $\mathbf{x}_u$ and $\dot{\mathbf{x}}_u$. Then the UMP is applied and a second simulation of 1 s is ran using $\mathbf{x}_0 = \mathbf{x}_u$ and $\dot{\mathbf{x}}_0 = \dot{\mathbf{x}}_u$. Once again the displacement and velocity vectors of the last time step are stored as $\mathbf{x}_U$ and $\dot{\mathbf{x}}_U$. Finally, the simulation here presented lasts 5 s, the time step Δt is assumed to be 10^{-5} s and the initial conditions are $\mathbf{x}_0 = \mathbf{x}_U$ and $\dot{\mathbf{x}}_0 = \dot{\mathbf{x}}_U$.

For the sake of brevity the orbits of only some nodes of the generator are shown. In particular, the orbits of the nodes corresponding to the bearings are considered to be more significant, since on the real machines vibration measuring planes usually corresponds to the bearing positions (figure 8). Moreover also the orbit of a node in the slotted part (node 18) of the rotor is shown in Figure 9. Note that the vibrations, and the orbits too, are referred to the centreline of the shaft, i.e. they do not consider the offset.

The orbits, shown in Figure 8 and Figure 9, are rather elliptical in the generator bearings, while are practically circular in the middle part of the generator. Moreover they are not fixed in the space but evolve

around a limit cycle, which is practically an attractor. A superficial analysis of the orbits could suggest that horizontal and vertical vibrations have only synchronous harmonic component in their spectra, but this opinion should be corrected once vibration spectra are considered.

The spectra in Figure 10 and Figure 11, namely those of the vibrations in the bearings and in the middle of the generator slotted part, show the synchronous component (50 Hz) as the main one and also the presence of a 2X component at 100 Hz. Anyhow, 2X harmonic component is very small with respect to 1X component, and this confirms the observation made in the previous chapter about the mode at 100 Hz.

However also a super-synchronous component at 71.6 Hz is evident and a rich sub-harmonic spectrum is present with the higher component at 21.6 Hz, which is greater than the 2X component. The last fact indicates high energetic content in sub-synchronous vibration that explains the dynamical behaviour of the system around the attractor shown in Figure 8 and Figure 9. Moreover, the presence of sub- and super-synchronous components, which are not integer multiple of the rotating speed, indicates the non-linearities introduced in the system behaviour by the UMP.

The presence of non-linearites is confirmed also by the analysis of the UMP spectra, shown in figure 12-figure 15. Besides the presence of 1X and 2X harmonic components, the super-harmonic component at 71.6 Hz is more evident than in the vibration spectra. In regards to the sub-harmonic components, once again the spectra are very rich and two components are more evident: the highest at 21.6 Hz and a secondary one at 28.6 Hz.

Note that traditional models dealing with UMP in generators, like [20] [21], do not allow emphasizing the presence of 1X force component, nor the presence of non-linearity.

Table 2 shows the magnitude of UMP forces. It is interesting to note that the total of the not-rotating pull force is about 33431 N that can be compared with the weight of the generator equal to 519781 N. The not-rotating pull force determines that the rotor orbits are moved with respect to the rotor centreline.

The other harmonic components can be compared with the unbalance, which is 98596 N. Moreover, the sub-synchronous component at 21.6 Hz is sensibly greater than the 2X component, underlying the relevance of non-linear effects in the UMP phenomenon.

The last confirmation of the presence of non-linear effects in the UMP is made by simulating the dynamical behaviour of the considered generator without the presence of the magnetic pull. The Newmark method is used again and in the eq. (36), that represents the excitation force, the only terms different from zero are those corresponding to the unbalance. The initial conditions were $\mathbf{x}_0 = \mathbf{x}_u$ and $\dot{\mathbf{x}}_0 = \dot{\mathbf{x}}_u$. Similarly, the simulation lasts 5 s and the time step Δt is assumed to be 10^{-5} s.

Figure 16 shows the orbit in bearing #1 that can be compared with figure 8. Also in this case the vibrations are referred to the centreline. The orbit shape is comparable even if the amplitude is little minor (due to the fact that UMP introduces an additional 1X force to the unbalance), but in this case the orbits are rather precisely superposed. The comparison between the 1X filtered orbits of the two cases is shown in Table 3 for node of bearing #1.

Table 2. UMP force magnitudes.

	Not-rotating force[(1)] [N]	Not-rotating resultant[(1)] [N]	1X - synchronous component (50 Hz) [N]	2X component (100 Hz) [N]	Super synchronous component (71.6 Hz) [N]	Sub synchronous component (21.6 Hz) [N]
$F_{x,UMP}^{(16)}$	–1837.39	8101.52@–103.11°	5284.41	28.21	4.36	158.33
$F_{y,UMP}^{(16)}$	–7890.42		5404.68	60.85	4.33	219.63
$F_{x,UMP}^{(17)}$	–1788.95	7569.03@–103.67°	3163.64	10.00	2.80	160.65
$F_{y,UMP}^{(17)}$	–7354.58		3220.70	22.21	2.89	223.77
$F_{x,UMP}^{(18)}$	–1918.17	8087.21@–103.72°	1847.05	3.37	1.89	152.29
$F_{y,UMP}^{(18)}$	–7856.44		1857.45	7.98	2.09	212.32
$F_{x,UMP}^{(19)}$	–2245.28	9674.15@–103.42°	970.18	0.74	1.36	133.24
$F_{y,UMP}^{(19)}$	–9409.99		950.09	2.04	1.64	185.41

(1) Not-rotating force component in *x* and *y* direction and resultant are referred to the reference system S'' of figure 4.

Table 3. Comparison of the generator 1X filtered orbits w/ and w/o UMP in bearing #1.

	Major axis amplitude [μm]	Major axis inclination [degrees]
W/ UMP	16.779	73.33°
W/o UMP	14.107	74.30°

Moreover, the centre of the orbit corresponds to the centreline, contrary to the previous case, since not-rotating components of the magnetic pull force are not present. The absence of non-linearities in this case is confirmed by the vibration spectrum, shown in figure 17 for the same bearing. The synchronous component is the only one evident and no sub- or super-synchronous are present. Similar results are obtained for the other generator nodes.

CONCLUSIONS

The phenomenon of the Unbalanced Magnetic Pull represents one of the most interesting cases in the electrical power generation machines, as they require a modelling both from the mechanical and electric point of view. In the present paper, a rather sophisticated model is introduced to calculate the magnetic pull in generators, which starts from the exact determination of the distribution of the air-gap, and then defines, by means of Maxwell stress calculation, the constant and dynamic forces that are caused by the asymmetric distribution of the air-gap. An application is introduced on a smooth generator of 320 MVA turbo-generator, operating at 3000 rpm, whose dynamic behaviour is simulated in the time domain. The results show that the magnetic pull in generators, besides the not rotating component, has 2X harmonic component, as can also be obtained by simplified models. Moreover, contrary to the simplified models, this method also displays a synchronous harmonic component and sub- and super- synchronous components, which indicate the non-linearity of this kind of excitation in the dynamic behaviour of the rotor.

REFERENCES

[1] Zawoysky RJ and Tornroos KC, "GE generator rotor design, operational issues and refurbishment options", *GE power System Report*, GER 4212, 08/01, 1-28.

[2] Nilsson LRK, "On the Vibration Behaviour of a Cracked Rotor", Proc. of *IFToMM Intl. Conf. Rotordynamic Problems in Power Plants*, Sept.-Oct. 1982, Rome, Italy, 515-524.

[3] Passleva G and Pira G, "Cracked shaft vibration sensitivity to steam temperature variations", Proc. of *IFToMM Intl. Conf. Rotordynamic Problems in Power Plants*, Sept.-Oct. 1982, Rome, Italy.

[4] Pennacchi P, Bachschmid N, Vania A, "A model-based identification method of transverse cracks in rotating shafts suitable for industrial machines", *Mechanical Systems and Signal Processing*, doi:10.1016/j.ymssp.2005.04.005.

[5] Frosini L and Pennacchi P, "Detection and modelling of rotor eccentricity in electrical machines: an overview", Proc. of *IMechE 8th International Conference on Vibrations in Rotating Machinery*, 7-9 September 2004, Swansea, Wales, 501-510.

[6] Bradford M, "Unbalanced magnetic pull in a 6-pole induction motor", Proc. IEE, 115(11), 1968, 1619-1627.

[7] Binns KJ and Dye M, "Identification of principal factors causing unbalanced magnetic pull in cage induction motor", Proc. IEE, 120(3), 1973, 349-354.

[8] Belmans R, Vandenput A, Geysen W, "Influence of unbalanced magnetic pull on the radial stability of flexible-shaft induction machines", IEE Proceedings Part B, 134(2), March 1987, pp. 101-109.

[9] Dorrel DG, Smith AC, "Calculation of U.M.P. in induction motors with series or parallel winding connections", IEEE Transactions on Energy Conversion, 9(2), June 1994, pp. 304-310.

[10] Dorrell DG, "The influence of rotor skew on unbalanced magnetic pull in cage induction motors with eccentric rotors", Proc. of *Electrical Machines and Drives*, 11-13 September 1995, pp. 67-71.

[11] Smith AC and Dorrel DG, "Calculation and measurement of unbalanced magnetic pull in cage induction motors with eccentric rotors. Part 1: Analytical model", IEE Proc.-Electr. Power Appl., 143(3), May 1996, 193-201.

[12] Smith AC and Dorrel DG, "Calculation and measurement of unbalanced magnetic pull in cage induction motors with eccentric rotors. Part 2: Experimental investigation", IEE Proc.-Electr. Power Appl., 143(3), May 1996, 202-210.

[13] Dorrel DG, "Calculation of unbalanced magnetic pull in small cage induction motors with skewed rotors and dynamic rotor eccentricity", IEEE Transactions on Energy Conversion, 11(3), Sept 1996, 483-488.

[14] Dorrel DG, Thomson WT and Roach S, "Analysis of airgap flux, current, and vibration signals as a function of the combination of static and dynamic airgap eccentricity in 3-phase induction motors", IEEE Transactions on Industry Applications, 33(1), Jan/Feb 1997, 24-34.

[15] Dorrel DG, "Experimental behaviour of unbalanced magnetic pull in 3-phase induction motors with eccentric rotors and the relationship with tooth saturation", IEEE Transactions on Energy Conversion, 14(3), Sept 1999, 304-309.

[16] Arkkio A, "Unbalanced magnetic pull in cage induction motors with asymmetry in rotor structures", Proc. of EMD97, 1997, 36-40.

[17] Holopainen TP, Tenhunen A, Arkkio A, "Electromechanical interaction in rotordynamics of cage induction motors", Journal of Sound and Vibration, 284(3-5), 2005, 733-755.

[18] Nabil AAN, Toliyat HA, "A novel method for modeling dynamic air-gap eccentricity in synchronous machines based on modified winding function theory", IEEE Transactions on Energy Conversion, 13(2), June 1998, 156-162.

[19] Toliyat HA, Nabil AAN, "Simulation and detection of dynamic air-gap eccentricity in salient-pole synchronous machines", IEEE Transactions on Industry Applications, 35(1), January/February 1999, 86-93.

[20] Stoll RL, "Simple computational model for calculation the unbalanced magnetic pull on a two-pole turbogenerator rotor due to eccentricity", IEE Proc.-Electr. Power Appl., 144(4), July 1997, 263-270.

[21] Guo D, Chu F and Chen D, "The Unbalanced Magnetic Pull and its Effects on Vibration in a Three-Phase Generator with Eccentric Rotor", *Journal of sound and Vibration*, 254(2), 2002, 297-312.

[22] Gustavsson RK and Aidanpää J-O, "The influence of Magnetic Pull on the Stability of Generator Rotors", paper ISROMAC10-2004-101, Proc. of The *10th Intl. Symposium on Transport Phenomena and Dynamics of Rotating Machinery*, Honolulu, Hawaii, March 7-11, 2004, 1-9.

[23] Kim KT, Kim KS, Hwang SM, Kim TJ, Jung YH, “Comparison of magnetic forces for IPM and SPM motor with rotor eccentricity”, IEEE Transactions on Magnetics, 37(5), September 2001, 3448-3451.
[24] Frosini L, Mimmi G and Pennacchi P, “Experimental analysis of rotor eccentricity in brushless motors”, Proc. of *11th World Congress in Mechanism and Machine Science*, Tianjin, China, 1-4 Aprile 2004, 5, 2095-2100.
[25] Rao SS, Mechanical vibrations, 4th Ed., Prentice Hall, 2003.
[26] Ivanov-Smolensky A, Electrical machines, vol. 1, Mir Publisher, Moscow, 1982.
[27] Brown DR and Hamilton EP, Electromechanical Energy Conversion, Macmillan Publishing Company, New York, 1984, 149-157.
[28] Chapman CR, Electromechanical Energy Conversion, Blaisdell Publishing Company, 1965, 91-95.
[29] Bachschmid N and Diana G, “Reduction of twice per revolution vibration levels due to weight effect in large turbogenerators”, Proc. of *IMechE Second International Conference Vibration in Rotating Machinery*, Churchill College, Cambridge, 2-4 Sept 1980, 203-208.
[30] Bachschmid N and Frigeri C, “Some results on the twice-per-revolution balancing of generators”, Proc. of *IFToMM International Conference Rotordynamic Problems in Power Plants*, Rome, 28 Sept- 1 Oct 1982, 49-54.
[31] Bachschmid N and Pennacchi P, “Subtask 4.6 – Polar Stiffness Asymmetry Model”, Brite EuRam Project No BE95-2015 “MODIAROT”, Contract No BRPR-CT95-0022, 1999, 1-7.
[32] Someya T, Journal-Bearing Databook, Springer-Verlag, 1989.
[33] Lalanne M and Ferraris G, Rotordynamics Prediction in Engineering, John Wiley & Sons Inc, Chichester, England, 1998.
[34] Pennacchi P, Bachschmid N, Vania A, Zanetta GA and Gregori L, “Use of modal representation for the supporting structure in model-based fault identification of large rotating machinery: part 1—theoretical remarks”, *Mechanical Systems and Signal Processing*, doi:10.1016/j.ymssp.2004.11.006.

LIST OF FIGURES:

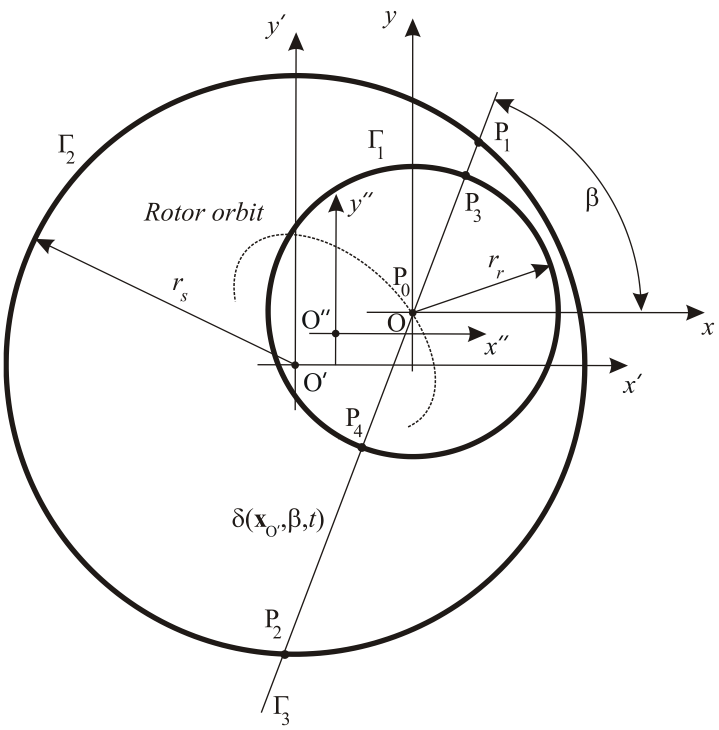

Figure 1. Calculation of the air gap length $\delta\left(\mathbf{x}_{O'},\beta,t\right)$.

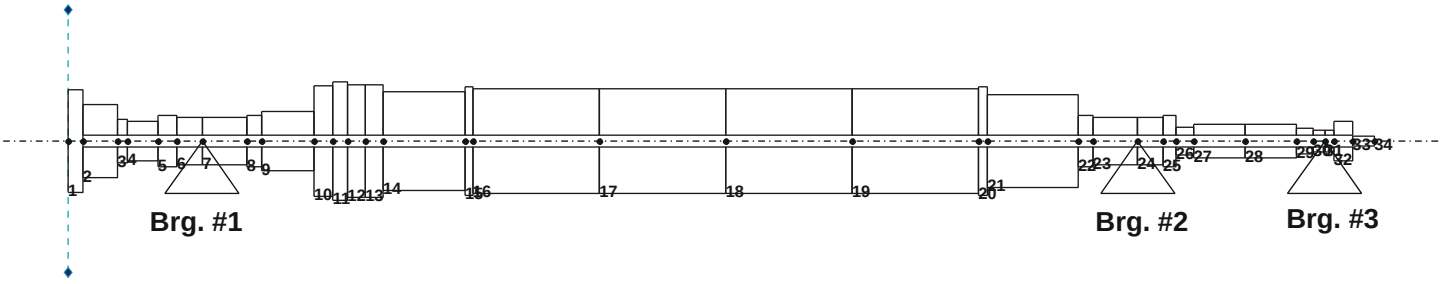

Figure 2. Generator model (mass diameters).

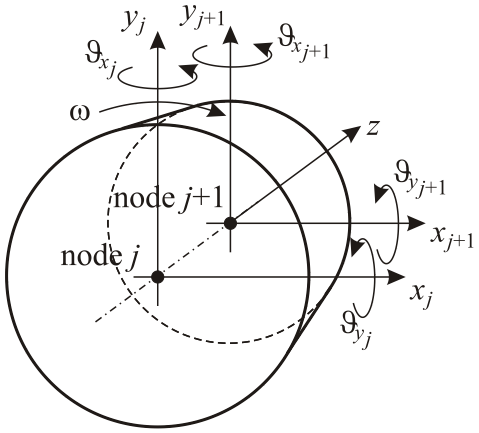

Figure 3. Reference systems of a general rotor element.

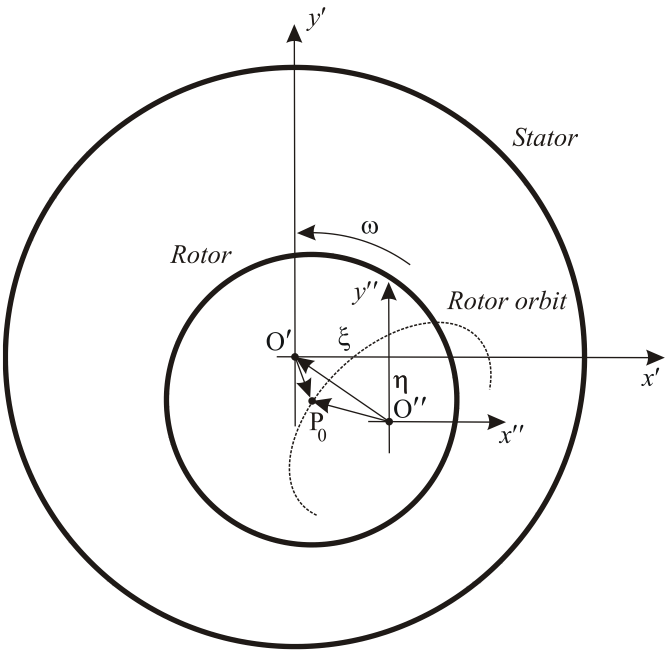

Figure 4. Rotor and stator relative positions.

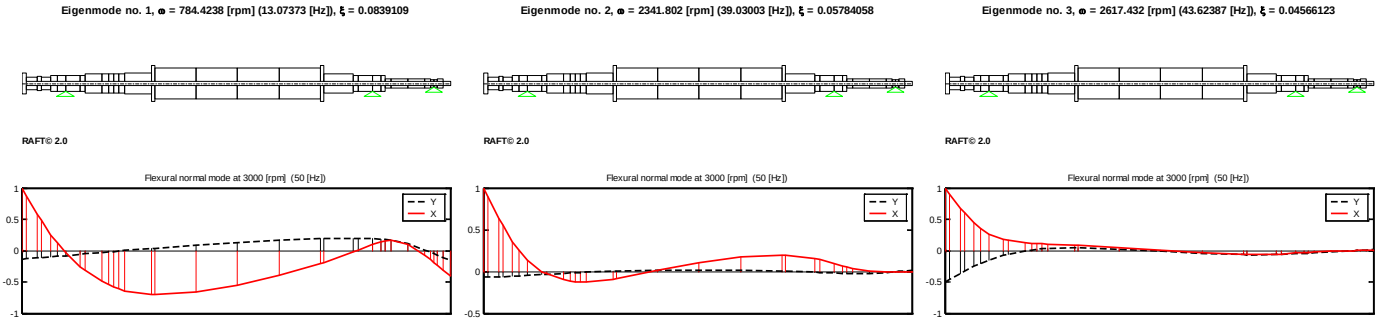

Figure 5. Normal modes below 50 Hz.

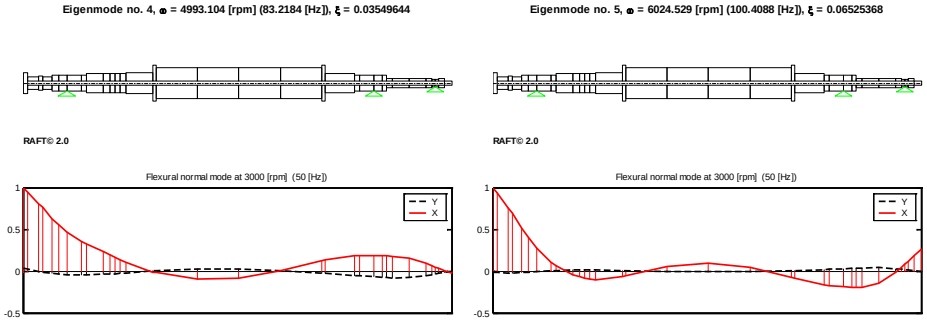

Figure 6. Normal modes over 50 Hz.

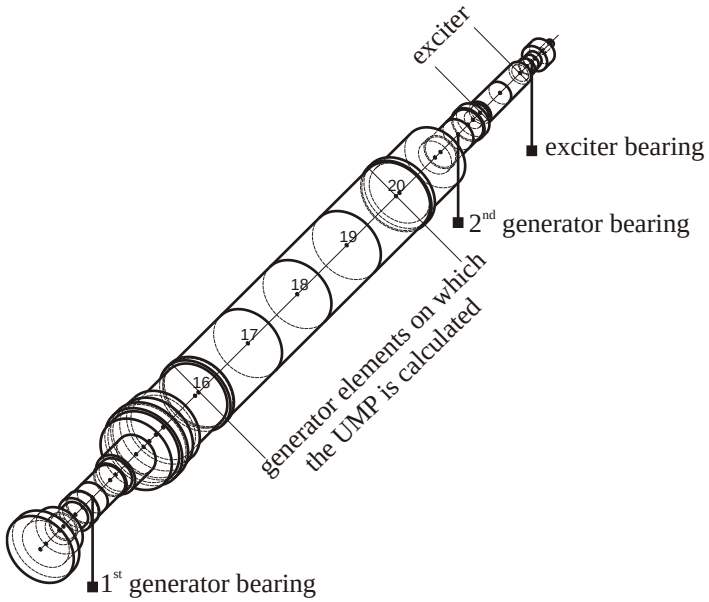

Figure 7. Generator elements on which the UMP is calculated.

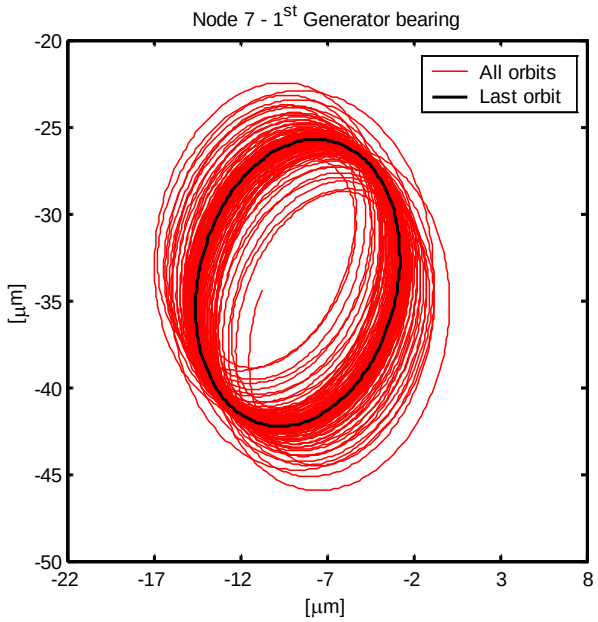

Figure 8. Rotor orbits in brg. #1.

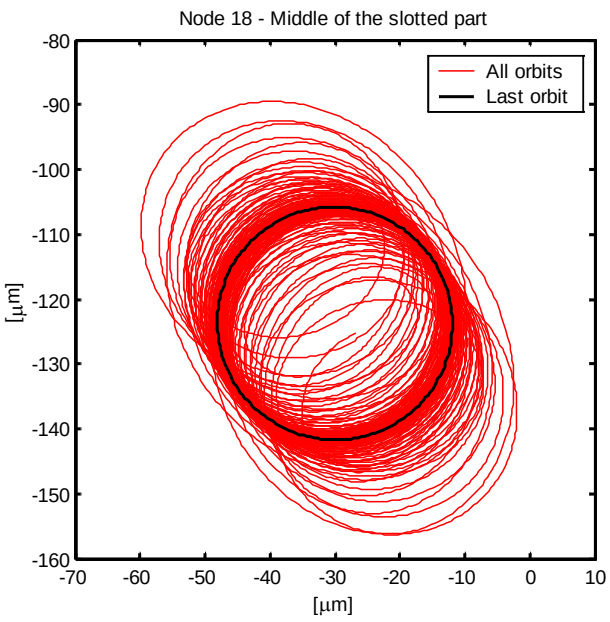

Figure 9. Rotor orbits in the middle of the slotted part.

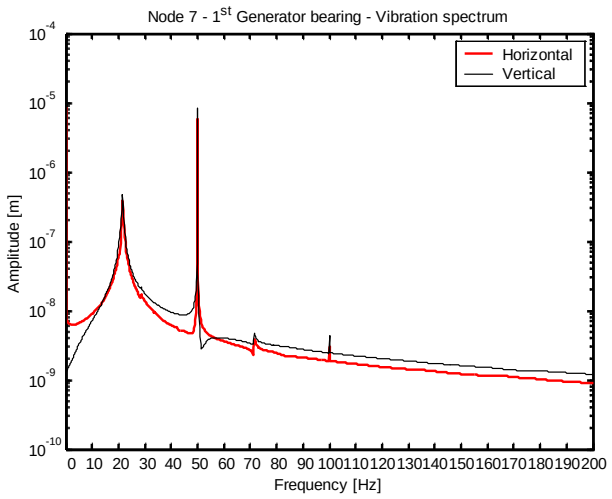

Figure 10. Vibration spectrum in brg. #1.

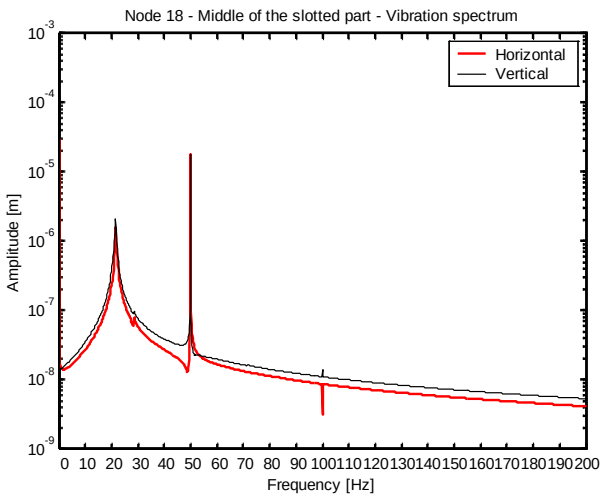

Figure 11. Vibration spectrum in the middle of the slotted part.

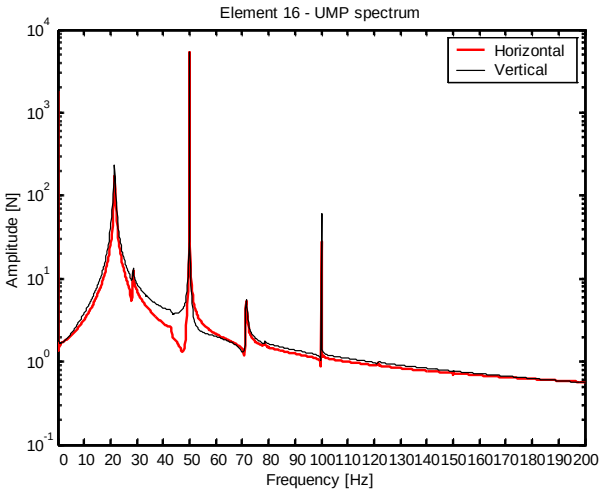

Figure 12. UMP spectrum on element 16.

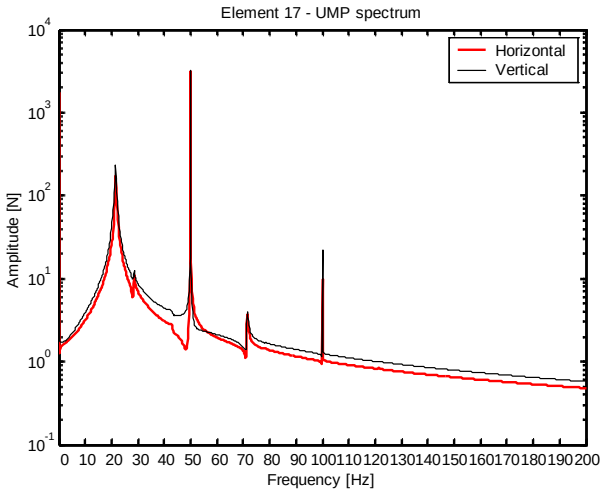

Figure 13. UMP spectrum on element 17.

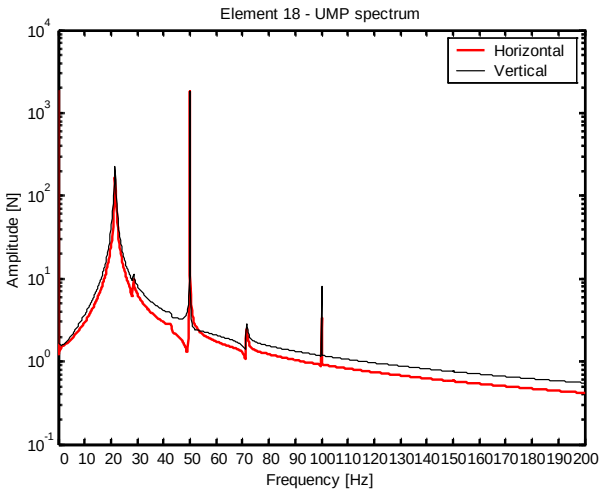

Figure 14. UMP spectrum on element 18.

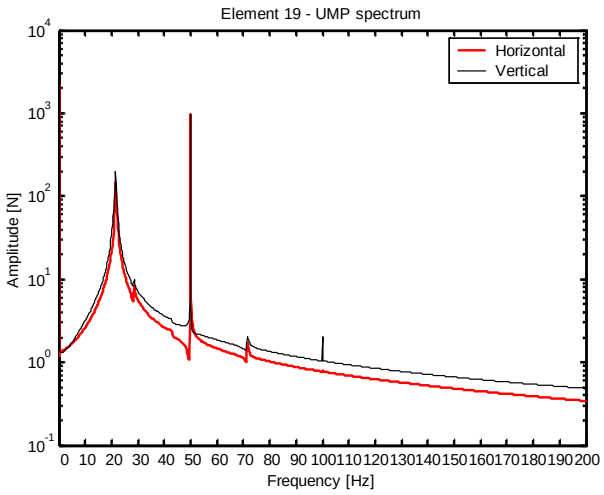

Figure 15. UMP spectrum on element 19.

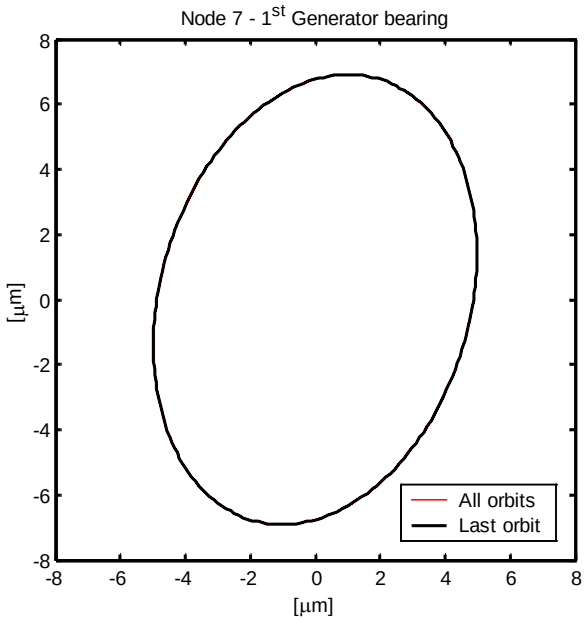

Figure 16. Rotor orbits in brg. #1 due to unbalance only.

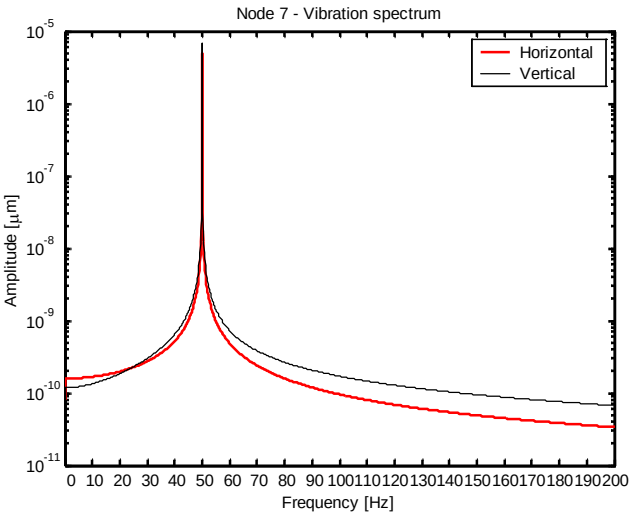

Figure 17. Vibration spectrum in brg. #1 due to unbalance only.